nature synthesis

Review article

https://doi.org/10.1038/s44160-026-01033-4

Synthetic routes to advancing perovskite solar cells through interface design

Received: 8 June 2025

Accepted: 24 February 2026

Published online: 16 April 2026

Check for updates

Jin Hou[1,3], Isaiah W. Gilley[1,3], Taylor E. Wiggins[1,3], Cheng Liu[1], Yi Yang[1], Bin Chen[1] ✉, Mercouri G. Kanatzidis[1] ✉ & Edward H. Sargent[1,2] ✉

Since the first demonstration in the early 2010s, perovskite solar cells (PSCs) have emerged as a promising next-generation photovoltaic technology. With power conversion efficiencies improving at a rate of approximately 1% per year, PSCs are approaching energy-efficiency parity with silicon-based photovoltaics. As single-junction efficiency gains begin to plateau, research efforts are increasingly directed towards addressing operating stability while maintaining device performance. Defects and impurities at the interface compromise long-term stability and limit device efficiency. Consequently, interface passivation has emerged as a central focus of the field. We emphasize three emerging strategies to improve how interfaces are constructed and engineered in PSCs: multifunctional passivation molecules suppress non-radiative losses and ion migration through cooperative interactions; heterostructure interfaces modulate band alignment and defect landscapes; and self-assembled monolayers offer molecular control over surface energetics and thin-film growth. These approaches target the root causes of performance loss and together tackle pressing topics in PSCs.

Given progress in efficiency, research on perovskite solar cells (PSCs) has turned to tackling questions relevant to real-world deployment and large-scale technological impact[1]. Whereas compositional optimization of the perovskite absorber layer is still ongoing, recent efforts have increasingly focused on interfacial engineering, as interfaces have emerged as key bottlenecks limiting long-term device performance[2,3]. In this context, rational interface design and the tailoring of interfacial functionalities using synthetic approaches are critical. These efforts aim to minimize interfacial charge losses, suppress degradation pathways and enhance overall device robustness[2,4,5].

In PSCs, interfaces between the absorbing layer and adjacent layers play a crucial role in dictating device efficiency and long-term stability. As charge carriers traverse the perovskite layer to adjacent transport layers, they encounter interfaces that often suffer from energetic misalignment, chemical incompatibility and defect-mediated recombination[3,6,7]. These regions, though physically thin, are chemically and electronically complex and substantially impact device performance under operational stress.

With interfacial engineering now a major focus in PSC development, we identify three emerging passivation strategies: multifunctional molecular passivation, heterostructure insertion and functional self-assembled monolayers (SAMs). These approaches can address the critical challenges associated with charge loss, degradation and device instability by targeting the complex interfaces between the perovskite and transport layers. A synthesis-centred overview of these three strategies is presented, exploring structure–property relationships, functional group requirements for defect-specific passivation, and intermolecular interactions.

Table 1 provides a comparative overview of the strategies discussed, listing representative reports of multifunctional molecular passivation, heterostructures and SAMs. It specifies the device interfaces for which each strategy is implemented, distinguishing modifications at the perovskite/electron transport layer (ETL) interface and/or perovskite/hole-transport layer (HTL) interface. It further summarizes reported power conversion efficiencies (PCEs), operational stability under maximum power point tracking at various

[1]Department of Chemistry, Northwestern University, Evanston, IL, USA. [2]Department of Electrical and Computer Engineering, Northwestern University, Evanston, IL, USA. [3]These authors contributed equally: Jin Hou, Isaiah W. Gilley, Taylor E. Wiggins. ✉e-mail: bin.chen@northwestern.edu; m-kanatzidis@northwestern.edu; ted.sargent@northwestern.edu

https://doi.org/10.1038/s44160-026-01033-4

Table 1 | Optimization focus and representative frontline reports for multifunctional molecular passivation, heterostructures and SAMs

Strategy	Applicable interface	Frontline report	PCE (%)	Operating stability	Performance improvement priority
Multifunctional molecular passivation	Perovskite/ETL and perovskite/HTL	79	26.30	MPP; 85 °C; T_{90}=1,100 h	PCE
		69	26.15	MPP; 65 °C; T_{90}=1,200 h	
Heterostructure	Perovskite/ETL and perovskite/HTL	131	25.40	MPP; 90 °C; T_{97}=3,670 h	Stability
		4	25.90	MPP; 85 °C; T_{91}=1,074 h	
		7	24.50	MPP; 55 °C; T_{99}=2,000 h	
SAM	Perovskite/HTL	100	26.92	MPP; 85 °C; T_{99}=1,000 h	PCE and stability
		194	26.30	MPP; 45 °C; T_{97}=2,000 h	

MPP, maximum power point.

temperatures, and designated performance improvement priority. Here performance improvement priority refers to whether a given strategy is principally aimed at maximizing the PCE, promoting long-term operational stability, or achieving concurrent optimization of both.

Perovskite synthesis

Halide perovskites exhibit a rich structural landscape, where variations in dimensionality, connectivity and composition profoundly influence their electronic structure, stability and transport properties. The interplay between these features enables rational design of materials with tailored optoelectronic behaviour across three-dimensional (3D), 2D and perovskite-related systems. These principles guide synthetic strategies and device architectures that continue to develop perovskite photovoltaic performance.

Types of perovskite light absorber

3D perovskites. 3D halide perovskites with the AMX_3 structure are the most widely studied and highest-performing class of perovskite light absorbers. In these materials, monovalent A-site cations such as methylammonium (MA^+), formamidinium (FA^+) or Cs^+ occupy the cuboctahedral voids formed by corner-sharing BX_6 octahedra, where M is typically Pb^{2+} or Sn^{2+} and X is a halide (I^-, Br^- or Cl^-)[8]. The $APbI_3$ composition exhibits a bandgap in the optimal range for single-junction photovoltaics (that is, ~1.5–1.6 eV), with high absorption coefficients (>10^5 cm^{-1})[9,10], allowing device thicknesses to be substantially shorter than mean carrier diffusion lengths. Together with their defect tolerance, these properties have allowed 3D PSCs to achieve certified PCEs exceeding 26%[1].

Compositional engineering plays an important role in tuning the bandgap and enhancing phase stability in 3D halide perovskites. Halide substitution, such as replacing iodide with bromide, increases the bandgap, whereas partial substitution of Pb^{2+} with Sn^{2+} narrows it, enabling continuous bandgap tunability across a wide spectral range (~1.2 to >3.0 eV; Fig. 1) to meet diverse application requirements, particularly for tandem solar cells[10]. Modifications at the A site, particularly with FA^+, MA^+ and Cs^+, are commonly used to suppress structural instabilities and stabilize the perovskite phase, as seen in α-$FAPbI_3$, which readily converts to a low-dimensional non-perovskite δ phase unless Cs^+ and MA^+ are incorporated to preserve the desired structure and improve crystallinity[11,12].

2D perovskites. Incorporating bulky organic spacer cations slices the 3D AMX_3 perovskite along the ⟨100⟩ crystallographic plane to yield 2D perovskites $\left(A'_2A_{n-1}Pb_nX_{3n+1}\right)$ with alternating organic and inorganic layers[13]. The number of inorganic layers (n) between organic spacers directly impacts both electronic and structural properties. As n increases, the bandgap narrows from ~2.5 eV (n = 1) towards ~1.7 eV, approaching the 3D limit (Fig. 1)[14]. In addition to tunable optoelectronic properties, 2D perovskites exhibit enhanced material stability compared with 3D perovskites, particularly against moisture and phase degradation, due to the protective role of the organic spacers[15].

Perovskite-related materials. Beyond these perovskite archetypes, a growing number of perovskite-derived materials, including double perovskites ($A_2M'M''X_6$), vacancy-ordered perovskites (A_2MX_6) and perovskitoids, have been developed to overcome toxicity and material stability concerns[15–17]. Lead-free double perovskites, such as $Cs_2AgBiBr_6$, offer enhanced air stability and lower toxicity, but they typically have indirect bandgaps and low absorption coefficients[18]. Perovskitoids, which deviate from the ideal corner-sharing perovskite structure, retain corner-sharing connectivity within the framework while also incorporating edge and/or face sharing[19,20]. These systems often exhibit higher phase stability and greater structural diversity, although their wider bandgaps (>2.0 eV) currently limit photovoltaic implementation[20].

Synthesis of single-junction PSCs

The synthesis of perovskite devices encompasses the fabrication of each individual layer, representing a highly customized and integrated process tailored to the specific properties of the constituent materials. This process is further influenced by the intended application context, whether for laboratory-scale studies, which often aim to approach the theoretical efficiency limits, or for industrial-scale manufacturing, where scalability, reproducibility, process compatibility and cost become the primary considerations.

Laboratory settings. The common fabrication techniques in laboratory settings are solution-based methods (for example, spin coating and blade coating) and physical deposition (such as thermal evaporation and atomic layer deposition), particularly for achieving high-performance devices. For the perovskite layer, spin coating remains the dominant approach, although other solution-based methods such as blade and spray coating are also employed. Although these solution-based methods can result in greater defect densities than physical or vapour deposition methods[21], this can be addressed by slowing crystallization via additive and antisolvent engineering[22]. The choice of technique for the charge-transport layers (CTLs) depends largely on material solubility; soluble materials are typically solution processed using solvents compatible with the perovskite layer[7], whereas others require vacuum-based deposition techniques such as thermal evaporation. The solution processability of transport layers is generally considered advantageous due to its lower energy requirements and compatibility with simple, rapid fabrication steps alongside the perovskite layer. For metal electrodes, thermal evaporation remains the standard due to limited alternatives. Screen-printed electrodes, which are employed in Si photovoltaics, have been used for perovskites[23], but the high temperatures (≥150 °C) needed to cure the contact paste can damage PSCs. Pastes that cure under mild heating or room temperature

https://doi.org/10.1038/s44160-026-01033-4

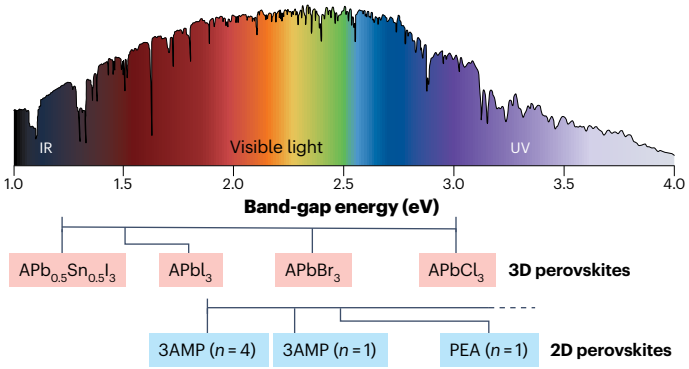

Fig. 1 | Band-gap energies of representative 3D and 2D metal halide perovskites aligned with the solar spectrum. 3D perovskites (red label shading), where A represents MA^+, FA^+ or Cs^+, span a broad portion of the solar spectrum. 2D iodoplumbates (blue label shading) are shown with varying layer thicknesses (n) and organic spacer molecules. $3AMP^{2+}$, 3-(aminomethyl) piperidinium; IR, infrared; PEA^+, phenethylammonium; UV, ultraviolet.

would be more applicable, but the challenge of screen printing onto PSCs without damaging or shunting the extremely thin (<1 µm) perovskite layer remains[24].

Industrial production. Spin coating is limited in scalability; solution-based techniques such as blade coating and printing are explored as candidate scalable approaches. A key challenge lies in translating well-established interfacial engineering strategies, such as molecular passivation and low-dimensional heterostructure integration, originally developed for spin-coated devices, to scalable manufacturing processes. This challenge arises primarily because surface passivation in perovskite devices is highly sensitive to both layer thickness and interfacial conditions[7,25]. Spin coating typically produces ultrathin, highly uniform and self-limiting passivation layers, enabled by rapid solvent evaporation and centrifugal thinning. In contrast, scalable methods such as blade or slot-die coating involve slower solvent removal and prolonged wet-film lifetimes, which can lead to less uniform passivation and altered interfacial reactions.

Furthermore, the surface characteristics of blade-coated perovskite films often differ markedly from their spin-coated counterparts in terms of roughness, residual additives and surface chemistry—attributes governed by coating kinetics, precursor composition and environmental conditions. Such variations critically influence how passivation molecules adsorb and react at the interface, ultimately shaping device performance and stability[26,27]. Given these considerations, methods that achieve interfacial passivation through direct incorporation into the perovskite precursor solution are particularly desirable[28,29]. Other strategies for improving the quality of slot-die-coated films include the use of a nitrogen air knife[27] and a laminar airflow dryer[30]. A comprehensive overview of large-area fabrication strategies is provided in a review by Liu et al.[31].

Synthesis for tandem and multi-junction cells

By integrating multiple absorbing layers with different bandgaps, multi-junction solar cells can surpass the theoretical efficiency limit of single junctions[32–34]. However, the successful fabrication of multi-junction solar cells imposes stringent requirements on synthetic methods, material design and device integration. Challenges, including Sn oxidation and phase segregation, plague perovskites at the narrow- and wide-bandgap regimens.

Narrow-bandgap perovskites. Perovskite bottom cells with narrow bandgaps are achieved through mixing Pb and Sn to produce mixed-metal compositions, with a minimum bandgap of approximately 1.2 eV around the $APb_{0.5}Sn_{0.5}I_3$ stoichiometry. This mixed composition has a narrower bandgap than either $APbI_3$ or $ASnI_3$ because it retains the low conduction band minimum resulting from the Pb $6p^0$ orbitals while raising its valence band maximum through the introduction of higher-energy Sn $5s^2$ orbitals[35]. This high-energy lone pair from Sn makes the mixed phase susceptible to $Sn^{2+} \rightarrow Sn^{4+}$ oxidation, the primary material stability concern of mixed PbSn perovskites. Whereas Sn oxidation in starting materials and precursor solutions is typically mitigated through atmospheric control or reversed through the inclusion of a reducing agent or Sn^0 metal[36,37], the oxidation of Sn in a working device is more difficult to curtail[38,39]. Ongoing work on narrow-bandgap perovskite device stability is primarily focused on additive engineering to control Sn oxidation in the film bulk[40] and interface engineering to control oxidation at the perovskite–HTL interface, where the acidic condition induced by a natural buildup of holes leads to accelerated oxidation of the perovskite layer[41]. One of the chief concerns is replacement of the common hole-transport material poly(3,4-ethylenedioxythiophene):poly(styrenesulfonate) (PEDOT:PSS) with other, less acidic HTLs. A summary of the operating stabilities of recently reported PEDOT:PSS-free PbSn devices is provided in the supplementary information of a recent paper by Bati et al.[42], and a salient historical overview and outlook on PbSn PSC stability is provided by Lee et al. in their 2023 review[43].

Wide-bandgap perovskites. Perovskite top cells with wide bandgaps are achieved by mixing Br and I to produce mixed-halide compositions. The widest regularly used bandgaps are approximately 2.0 eV with the $APb(Br_{0.67}I_{0.33})_3$ stoichiometry[44]. These mixed-halide compositions are plagued by light-induced halide segregation[45,46], a phenomenon in which the mixed phase segregates under illumination, resulting in I-rich regions of the thin film that absorb light intended for other sub-cells and trap charge carriers, hindering device performance. Strategies to mitigate this halide segregation have primarily focused on compositional and molecular additives that attenuate ion migration[47]. However, work by Rand and co-workers[48] has suggested that halide oxidation catalyses phase segregation, indicating that demixing within devices, like other forms of perovskite degradation, probably begins at perovskite–CTL interfaces. There does not exist consensus as to the precise driving force for halide segregation across mixed-halide perovskites. Proposed mechanisms include thermodynamic demixing[49], polaron-induced demixing[50] and the formation of mobile iodide vacancies[51,52]. As these mechanisms are not mutually exclusive, they may each play a role in halide segregation. Furthermore, as the rate, temperature dependence and reversibility of halide demixing depends on the precise halide composition[53–55], which of these mechanisms is dominant may vary with halide composition.

Molecular design for passivation

Molecular passivation has been widely adopted for interface optimization in PSCs. Applying a thin passivation layer on top of the perovskite can enhance the open-circuit voltage and fill factor by passivating surface defects and repelling minority charge carriers due to the enhanced band alignment, thereby boosting device efficiency. Simultaneously, the passivation layer acts as a barrier to ion migration, mitigating perovskite degradation and improving device stability[56,57].

Origin of performance loss at interfaces

Two primary issues at the interface between perovskites and CTLs undermine the performance of PSCs. The first is charge-carrier recombination, which occurs at the perovskite surface and across the perovskite/CTL interface. At the perovskite surface, defects originate primarily from precursor material impurities, rapid nucleation and growth during crystallization[58], as well as degradation under device operation[59]. The predominant surface defects are Lewis-acidic, electron-localizing traps (for example, under-coordinated Pb^{2+} ions) and Lewis-basic, hole-localizing traps (for example, under-coordinated

halides)[60]. At the perovskite/CTL interface, near-interface minority carriers (such as holes in the perovskite) recombine with majority carriers (electrons in the ETL) across the interface[25,61]. These recombination pathways reduce the device open-circuit voltage and fill factor, impairing the overall device efficiency.

The second critical issue is ion migration, which occurs both within the perovskite bulk and across the perovskite/ETL interface. At the interface, this irreversible migration is particularly problematic, as perovskite species have been observed to diffuse into the ETL and even into the electrode, leading to chemical corrosion and accelerated device degradation[62,63].

Functionalities of passivation molecules

To tackle these issues, molecular passivation strategies are typically designed to fulfil one or more of three primary functions: (1) chemically passivating surface defects on the perovskite; (2) repelling minority charge carriers; and (3) suppressing ion migration at the perovskite/ETL interface.

For surface defect passivation, the most employed molecules are Lewis acids and bases, selected based on the nature of the surface traps on the perovskite, as well as the adjacent transport layer. Lewis bases chemically passivate Lewis-acidic electron traps, whereas Lewis acids passivate Lewis-basic hole traps (Fig. 2a). Lewis bases used for passivation typically feature nitrogen-containing groups[64,65], carbonyl groups[66–68], organosulfur[65,69,70] or conjugated π systems[71–73]. In contrast, Lewis acid passivants typically contain electron-deficient atoms such as boron[74] or an oxidized metal (for example, Eu^{3+})[75], although normally basic atoms such as phosphorus[76] and iodine[77] can be rendered Lewis acidic when functionalized with extremely electron-withdrawing groups, such as pentafluorophenyl moieties. At the perovskite/ETL interface, where electrons are the primary charge carriers being extracted, passivating electron traps with Lewis bases can effectively suppress non-radiative recombination and enhance electron extraction, offering greater benefits than targeting hole traps. It follows that Lewis acids, while less commonly used, may be particularly effective at the perovskite/HTL interface, serving a similar role by passivating hole traps.

Field-effect passivation strategies, which aim to repel minority carriers from the interface (such as holes at the perovskite/ETL interface), utilize ions to electrically repel like-charged carriers. Cations used for field-effect passivation typically contain ammonium or amidinium groups[78–81], whereas common anionic moieties are carboxylate, sulfate and phosphate groups[69,82–85]. As anions repel electrons and cations repel holes, their use is largely limited to the HTL and ETL interfaces, respectively.

To suppress ion migration, in addition to coordinating with surface defects, several molecular design strategies are commonly employed: (1) introducing hydrogen-bonding groups (for example, –OH and –COOH) that bind to halide ions and immobilize them[86,87]; (2) depositing a compact metal oxide layer[88,89]; and (3) utilizing cross-linkable units to form robust networks that block ion migration pathways and reduce defect formation[90,91].

Multifunctional passivation

Considering their ability to coordinate defects and repel minority carriers, we classify these passivating molecules into four overlapping categories: Lewis bases, Lewis acids, cations and anions (Fig. 2a). Molecules positioned at the intersection of these categories exhibit multifunctional properties, enabling synergistic passivation effects (Fig. 2b, right). This multifunctionality can also be achieved by the application of multiple molecules from these different categories (Fig. 2b, left). Previous studies have demonstrated substantially performance improvements enabled by such multifunctional strategies[25,79,81,85]. For instance, at the top interface (perovskite/ETL), a well-designed molecule can simultaneously promote electron extraction while repelling holes[25]. This multifunctional passivation approach has become an increasingly prominent trend in recent research.

Multifunctional unary passivants. The most widely adopted multifunctional passivation strategy involves incorporating various functional groups into a single molecule, with each group targeting and passivating specific defects. For example, a molecule containing both an ammonium group and a thiol group can simultaneously passivate A-site cation vacancies and under-coordinated Pb^{2+} ions, respectively[92]. Building on defect passivation, additional functional groups, such as halogens, can be introduced into the molecular structure to regulate film formation and enhance perovskite crystallinity[69,93]. Furthermore, passivant molecules can be designed to be cross-linkable, forming a robust network that provides additional benefits, such as improved passivation effectiveness, enhanced hydrophobicity and stronger barriers to ion migration[94].

Multimolecular passivation. For multimolecular passivation, several considerations and design scenarios have been explored. First, individual passivants can function independently, each contributing to improved device performance. For example, Liu et al.[25] employed a bimolecular strategy in which a methylthio-containing molecule passivated defects while a diammonium molecule repelled minority carriers and suppressed non-radiative recombination, collectively enhancing the solar cell efficiency compared with conventional single-ammonium passivation[25].

A more recent and increasingly popular approach involves either synergistic passivants, where one enhances the effect of the other, or cooperative passivants, which complement each other by targeting different types of defects. For instance, conventional ammonium-based passivants often suffer from poor charge transport, unfavourable molecular orientation and weak binding with the perovskite surface. To address these issues, a secondary boosting agent such as a halogenated molecule[95] can be introduced alongside the ammonium passivant to improve the transport properties of the passivation layer and strengthen the passivant–perovskite binding, thereby amplifying the overall passivation effect[95–98].

Buried-interface passivation

Owing to the sequential nature of perovskite device fabrication, the bottom interface serves as the foundation for perovskite film formation. Therefore, it requires particular attention to surface wettability and energy-level alignment to ensure uniform, highly crystalline films and efficient charge extraction.

Considerable efforts in the field have focused on integrating molecular passivation with conventional hole-transport materials. For instance, Chen and co-workers[99] employed multiple aromatic carboxylic acids to enhance the surface wettability of SAMs. Jen and co-workers[100] introduced an azide-containing molecule capable of crosslinking with SAMs to form co-SAM structures that markedly strengthen interfacial adhesion and improve operational stability.

Molecular passivation at the buried interface is particularly impactful in tin-based narrow-bandgap PSCs. In such compositions, the commonly used SAMs for single-junction devices often exhibit energy-level mismatch with typical hole-transport layers such as the water-based PEDOT:PSS. However, the strong acidity of PEDOT:PSS can degrade tin perovskites; acidity control using ammonia-containing molecules has shown great promise in improving interfacial stability[101,102]. Moreover, amines with dipole have been employed to further tune the energy alignment at the buried interface, thereby increasing the open-circuit voltage of tin halide perovskites[103]. Molecular passivation has also been effectively combined with other HTLs such as NiO_x, for similar purposes mentioned above[104,105].

Overall, the multifunctional passivation strategy is fundamentally superior to traditional unary approaches. In our view, this emerging

https://doi.org/10.1038/s44160-026-01033-4

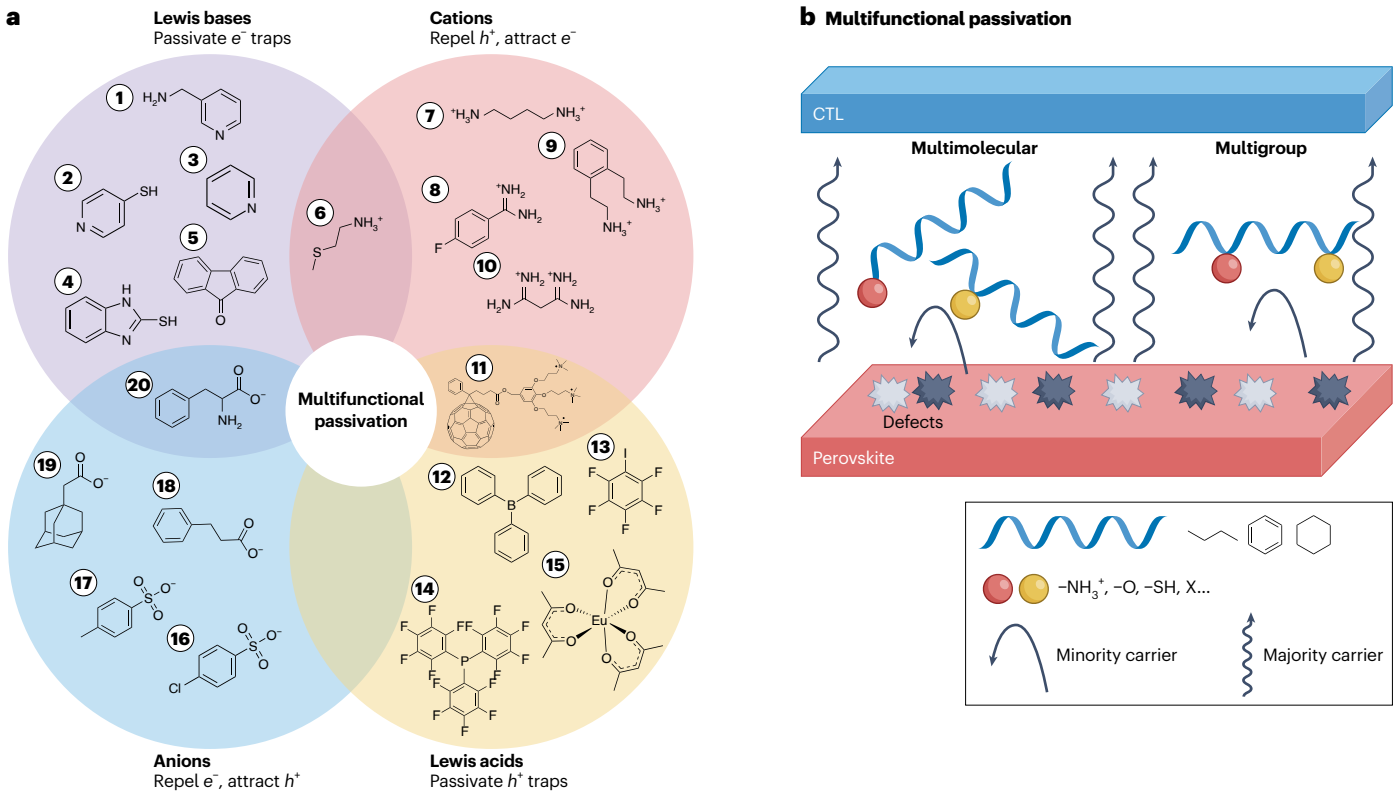

Fig. 2 | Molecular classification and working mechanism of multifunctional passivation. a, Common molecule classes used in multimolecular PSC passivation. Molecules **1**–**6**, **7**–**11**, **12**–**15** and **16**–**20** are reported in refs. 25,64–66,71, refs. 78–81, refs. 74–77 and refs. 69,82–85, respectively. **b**, Working principle of the multifunctional passivation strategy, illustrating two complementary mechanisms: chemical passivation, which neutralizes defects; and field-effect passivation, which repels minority carriers.

method holds the key to the future development of PSCs and should be a primary focus for future research in the field. However, we note that the improvements from this strategy so far are mainly in efficiency, and issues related to long-term molecular stability persist. Particularly, many passivation molecules themselves lack sufficient thermal robustness and may degrade at elevated temperatures. Therefore, improving the intrinsic stability of the passivating agents will be crucial for future investigations[25,79,106].

Heterostructure construction

The poor interfacial stability of perovskite–CTL interfaces motivates the insertion of additional, more stable layers between the perovskite and adjacent CTLs to passivate interfacial defects and improve device efficiency and stability. Such additional layers can comprise perovskites, perovskite-related materials or entirely different materials, and the resulting heterostructure can comprise a gradual (graded) or sharp (bilayer) transition between the two layers, inserted at the buried or top interface. In each case, the added operating stability from heterostructure insertion must be balanced against impacts to charge transport, so the bandgap, band alignment and thickness of the inserted layer are important considerations.

Band alignment and charge transport

Because the charges pass through the inserted material before extraction, it is important to consider the band alignment of the inserted layer with the absorber and CTL. In an ideal case, the inserted layer would have a type II (staggered) band alignment relative to the perovskite absorber, with the relevant band extremum lying between the perovskite and its CTL (Fig. 3a). In such a case, the desired charge carrier would experience a minimal energetic barrier passing through the heterostructure, and the undesired charge carrier would be repelled. However, many inserted materials lack this ideal band alignment, and a misaligned layer can potentially act as a barrier or trap. In cases with non-ideal band alignments or in which the inserted layer has low mobility for the desired carrier, the thickness of the inserted material will determine the extent to which charge extraction is attenuated. Even extreme band misalignment can have a negligible effect on charge extraction if the inserted layer is thin enough for carriers to tunnel past it (Fig. 3b).

Heterostructure materials

A unifying property of inserted materials is that they are more stable than the underlying 3D perovskite. These inserted materials are commonly compositionally related to perovskites, including 2D perovskites, perovskitoids and other perovskite-related materials, but unrelated materials are also used. For example, 2D perovskites and low-dimensional perovskite-related materials are inserted by spin coating a solution of their spacer cation dissolved in isopropanol, in which the 3D perovskite has weak solubility[107–110]. The addition of a stronger polar solvent, such as dimethylsulfoxide, or extensive post-treatment annealing causes further disruption of the underling perovskite, resulting instead in a gradient heterostructure[111–113].

Perovskites. As the PSC already contains a 3D perovskite absorber, 3D/3D perovskite heterostructures have primarily been used for particularly unstable perovskites, such as Pb–Sn narrow-bandgap[33] and mixed-halide wide-bandgap[114] absorbers. More commonly, 2D perovskites are inserted, for which the great variety of 2D-perovskite-forming organic cations and high degree of bandgap tunability are key advantages[115,116]. These advantages are particularly apparent in 2D perovskites with a high n value ($n \geq 3$), which tend to have natural type II band alignments with normal-bandgap (1.5–1.6 eV) 3D perovskites

https://doi.org/10.1038/s44160-026-01033-4

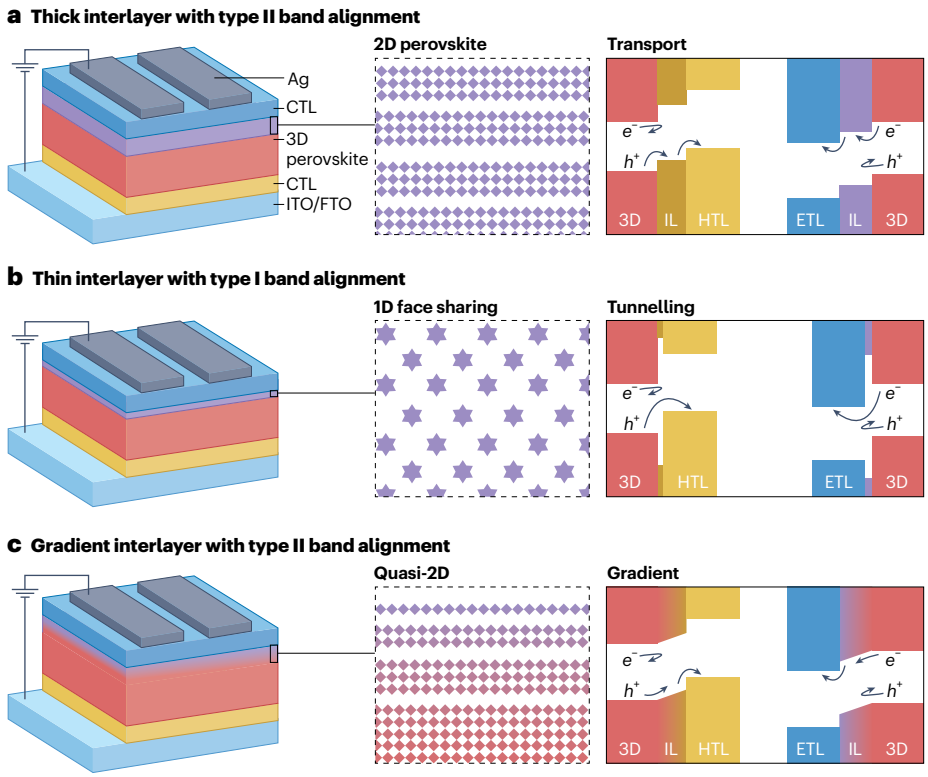

Fig. 3 | Common heterostructures and corresponding transport mechanisms. **a**, Schematic showing the structure of a PSC (left) with a thick 2D-perovskite inserted layer, represented by a stylized projection of the $n = 3$ crystal structure (middle; organic molecules omitted for clarity), and example band alignment showing charge transport through the inserted layer (right). **b**, Schematic of a structure with a thin 1D non-perovskite inserted layer, represented by a stylized projection of the δ-$FAPbI_3$ crystal structure, and band alignment showing tunnelling. **c**, Schematic of a structure with an inserted layer of gradient quasi-2D perovskite, represented by a stylized projection showing $n = 1$, 2 and 3 layers on top of a 3D perovskite, and band alignment showing gradient transport. FTO, fluorine-doped tin oxide; ITO, indium tin oxide; IL, interlayer.

(Fig. 3a)[107,117–119]. However, the highly anisotropic charge transport of 2D perovskites renders their orientation a primary concern when inserting a thick (>10 nm) layer[109]. Furthermore, the similar solubility of 2D and 3D perovskites in most solvents renders it difficult to cleanly deposit a layer of 2D on 3D or vice versa without partially dissolving the underlying layer, often producing a mixture of n values. Such perovskites are sometimes described as quasi-2D (Fig. 3c)[112,120]. Although there are examples of similar insertions with 1D perovskites[121], these are less commonly used due to their much wider bandgaps and unidirectional charge transport. Low-dimensional perovskitoids have also demonstrated potential as inserted layers with the ability to halt spacer cation migration[17].

Perovskite-related materials. 1D face-sharing non-perovskite phases represent another common type of inserted material[122–126]. As for 2D perovskites, these materials can typically be deposited using the same methods as 3D perovskites, making their insertion simple. Although they are highly air and water stable, these face-sharing materials tend to have very wide bandgaps (>2.5 eV) and poor charge transport, making them barriers to charge extraction. For this reason, inserted layers of such materials need to be thin enough to enable charge-carrier tunnelling (Fig. 3b).

Other materials. A variety of other, perovskite-unrelated, materials have been inserted into PSCs, including graphene[127], lead sulfide[128], molybdenum disulfide[129], aluminium oxide[130] and others, typically deposited by thermal evaporation, sputtering or atomic layer deposition. In contrast with the soft-lattice nature of 2D perovskites, these materials typically exhibit intrinsically more robust structures, which more effectively suppress ion diffusion across the interface, thereby contributing to some of the best demonstrations of device stability reported so far[3,131]. However, their efficiencies still lag behind those achieved with molecular passivation strategies, such as propane-1,3-diammonium iodide[48,88] or ethane-1,2-diammonium treatments[25,100], whose PCEs have already approached 27%.

Heterostructure grading

Most perovskite heterostructures with unrelated materials have a sharp transition between the two layers and are known as bilayer heterostructures (Fig. 3a,b). However, low-dimensional perovskites and related materials can mix with 3D perovskites, forming gradual transitions known as graded heterostructures (Fig. 3c)[112,113]. Such graded morphologies are particularly common in 2D/3D perovskite heterostructures, in which a gradient of n values is formed. These typically form because the solvents used to deposit 2D perovskites partially dissolve 3D perovskites, but recent work has shown that acetonitrile, propylene carbonate and tetramethylene sulfone preferentially dissolve 2D perovskites and have minimal solubility for 3D perovskites[7]. In other cases, careful choice of the 2D-perovskite spacer cations[110] or additional washing steps are necessary to ensure phase-pure 2D layers[132]. Although solvent choice governs the initial topology of the bilayer heterostructure, post-synthetic diffusion of organic cations is still possible. Thus, the long-term heterostructure stability depends on the spacer and cage cations and their relative ionic mobilities in the 2D and 3D phases.

As graded heterostructures inherently contain a concentration gradient of ions, they can encourage ionic diffusion across the heterostructure, especially for 2D/3D perovskite heterostructures[133,134].

This diffusion leads to a natural tendency for graded heterostructures to homogenize over time, sometimes rendering them less stable than bilayer heterostructures, at which the sharp boundary between layers can mitigate ion transfer between layers. This phase gradient can, however, assist in transporting charge or reducing strain across the heterostructure[112]. In one case, a gradient of halide composition counteracts the diffusion of iodide anions towards the surface of the perovskite, partially mitigating the effects of halide segregation[135]. In cases where the heterostructure is inserted at the buried interface, the formation of a bilayer becomes more difficult, as the solvents that dissolve 3D perovskites nearly universally dissolve 2D perovskites[7]. Although the emerging focus on operational stability for PSCs may render bilayer heterostructures more stable, specific applications of graded heterostructures, especially for wide- and narrow-bandgap perovskites and at buried interfaces, will remain impactful.

Heterostructure interface selection

The final consideration for inserted materials is at which interface to insert them. This choice is often dictated by the overall device architecture, which determines which charge carriers are extracted at the buried and exposed interfaces. Because most perovskite-related materials are readily dissolved by the solvents used for 3D perovskite deposition, it is difficult to fabricate a heterostructure at the buried interface without destroying the underlying layer[7,136,137]. For this reason, most heterostructures are inserted at the exposed interface[17,107–109,112,115,116,120–126,138]. Because most PSCs are fabricated in a p–i–n architecture, these exposed-interface heterostructures are typically inserted between the perovskite and ETL, so their alignment with the conduction band of the 3D perovskite is particularly important. Nevertheless, buried-interface insertion has been demonstrated[136,139,140], and a better understanding of the nucleation and growth kinetics of 2D perovskites has enabled single-step deposition of buried-interface 2D/3D heterostructures[141]. However, such heterostructures are typically graded and vulnerable to ion migration, so further work is necessary to access the fabrication of phase-pure buried-interface bilayer heterostructures.

Overall, although the construction of heterostructures generally offers a more robust approach than molecular passivation, careful consideration is required regarding the specific materials employed. For instance, when using 2D-perovskite capping layers, the selected 2D spacer should not penetrate the underlying 3D lattice, as this can compromise surface passivation[142]. Conversely, incorporating more rigid and compact non-perovskite materials can effectively mitigate ion migration but may also hinder charge transport, which results in lower efficiency gains compared with molecular passivation. Future development of this strategy should focus on the rational design and discovery of materials that preserve the structural robustness of the heterostructure while maintaining efficient charge transport, even in relatively thick layers.

Formation of SAMs

SAMs have emerged as a promising and molecularly tunable strategy for mitigating interfacial losses in PSCs. Although solution-processing methods such as dip coating, spin coating and spray coating are commonly used to deposit SAMs onto metal oxide surfaces, alternative approaches include vapour exposure, thermal evaporation and incorporation into the perovskite precursor solution[143]. By forming a single- or several-molecule-thick layer through spontaneous chemisorption on solid substrates, SAMs enable precise control over surface energetics, facilitate chemical passivation of interfacial defects and promote favourable perovskite growth without adding parasitic absorbance or resistive loss. Their molecular versatility makes them particularly compelling for p–i–n device architectures, where they are implemented at the bottom interface as hole-selective layers (Fig. 4a).

A key advantage of SAMs lies in their modular molecular nature, comprising three components: an anchoring group, a molecular linker and a terminal head group (Fig. 4b). Each component plays a distinct role in shaping the chemical and electronic landscape of the interface[144]. This collective functionality allows SAMs to simultaneously address multiple bottlenecks in perovskite photovoltaics, including device stability, charge extraction and perovskite crystallization.

Anchoring group

The anchoring group facilitates the interaction between the SAM and the substrate (typically a metal oxide such as SnO_2 or NiO_x) through covalent or coordinative bonds. The binding strength of common anchoring groups, such as phosphonic acid, carboxylic acid, boric acid, cyanovinyl acid and silane groups, is tied to their pK_a values, which govern their degree of deprotonation and thus their ability to form strong, stable bonds on metal oxide surfaces (Fig. 4c, right)[145]. Low-pK_a groups such as phosphonic acids anchor more robustly than higher-pK_a groups such as boric acids, whereas silanes form covalent siloxane (Si–O–Si) networks after hydrolysis[146,147]. It is also important to consider the long-term adhesion and hydrolytic stability of these anchoring groups under ambient conditions. Silane groups, though capable of forming covalent siloxane networks, are prone to hydrolytic degradation, and their polymeric framework must be carefully controlled to avoid forming a disordered, poorly packed siloxane layer that compromises interfacial integrity[148,149]. In contrast, phosphonic acids exhibit markedly higher hydrolytic resilience and interfacial binding[150]. Mechanistically, they initially absorb to the substrate via hydrogen bonding and subsequently undergo thermal annealing (condensation) to form covalent metal–oxygen–phosphorus bonds. Iterative cycles of deposition, annealing and washing to remove unbound molecules further promote the formation of a dense, well-ordered monolayer. In addition to strong adhesion, anchoring groups influence the molecular dipole by modulating electron density within the molecule. This tuning of the molecular dipole subsequently alters the energy levels of the substrate, enhancing its work function alignment with the perovskite, thus improving charge extraction and device performance.

The thermal and ultraviolet stability of SAMs is largely dependent on the molecular integrity of the monolayer and the chemical robustness of the anchoring group–substrate bond, where long-lived anchoring under environmental and photonic stress is directly correlated with the retention of device performance over time[151,152]. Phosphonic acids are currently the most widely used and effective anchoring groups due to their strong substrate binding through mono-, bi- or tridentate bonds, establishing them as the most effective and industrially viable motif developed to date[145,147,153–157]. However, some studies suggest that the strong acidity of phosphonic acids may lead to undesirable chemical interactions with the perovskite and underlying substrate[158,159]. As a result, research has begun to explore weaker acids, such as boric acid, which effectively reduces acidic degradation while maintaining strong adhesion under operational stress[160]. In n–i–p device architectures, recent work has explored the placement of SAMs on top of the perovskite layer. Lattice-matched anchoring groups enable epitaxial self-assembly of SAMs, aligning molecular dipoles with the perovskite lattice and contributing to defect passivation by interacting with under-coordinated surface sites[161]. Collectively, these strategies highlight the crucial role of anchoring groups in stabilizing the interface, but also actively tuning the electronic properties of PSCs.

Linker

The linker functions as the molecular bridge that connects the anchoring group to the terminal head group. Although it does not directly interface with the substrate or the perovskite, its chemical identity—whether rigid or flexible, conjugated or insulating—can strongly influence molecular orientation, packing density and monolayer ordering[162]. As such, linker design offers a subtle yet powerful strategy for tuning the function of the entire SAM.

https://doi.org/10.1038/s44160-026-01033-4

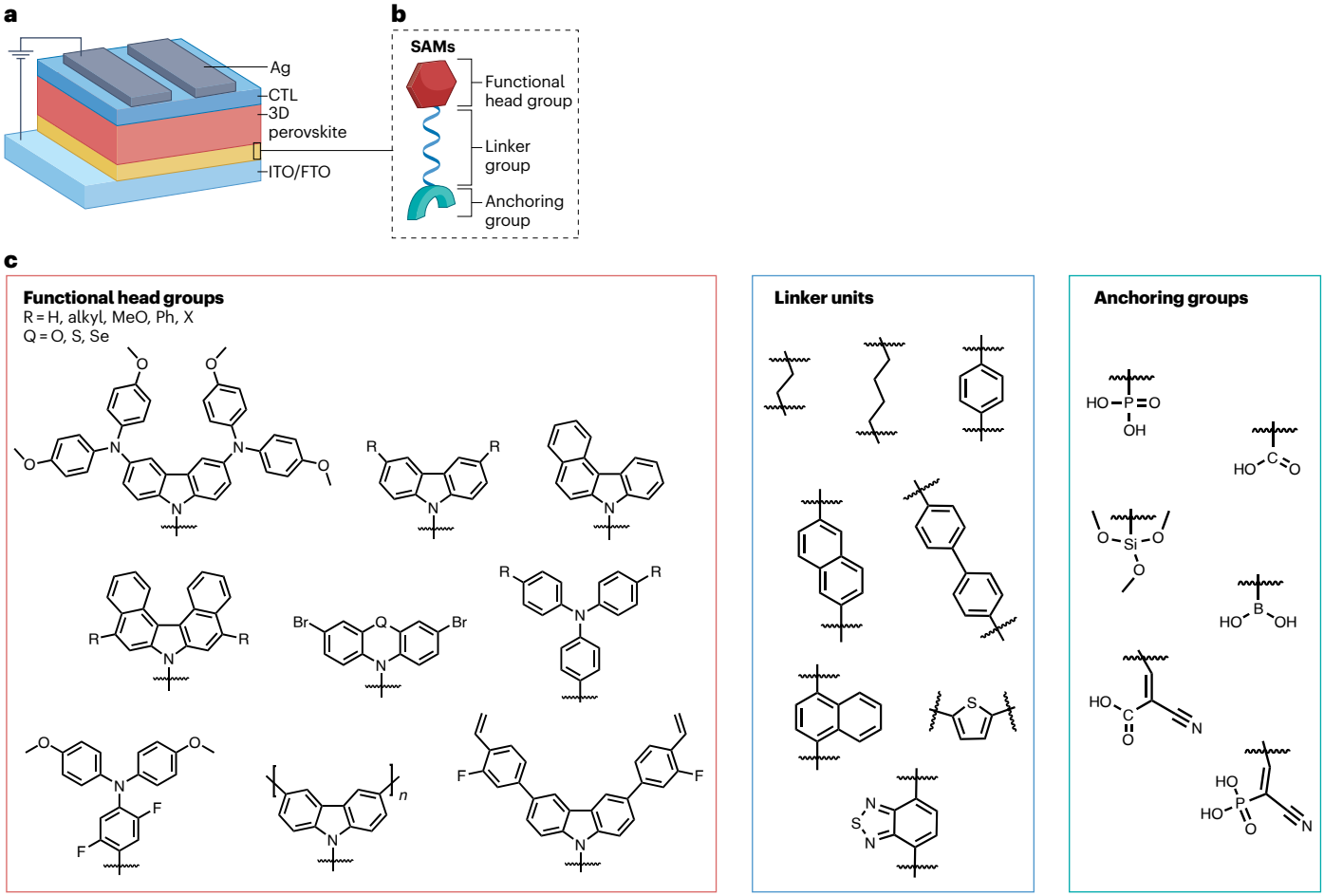

Fig. 4 | Functional SAMs for PSC passivation. a, Schematic of a PSC with an exaggerated SAM layer (orange). **b**, Schematic of the SAM components. **c**, Common functional head groups (left), linker units (middle) and anchoring groups (right) used in functional SAMs.

Initially, SAMs were predominantly based on alkyl chain linkers. However, the electronically inert nature of these chains limits their effect on interfacial energetics and charge-carrier dynamics[163]. To overcome these limitations, recent work has investigated aromatic linkers such as thiophene, thiadiazol, naphthalene and phenyl derivatives (Fig. 4c, middle)[164–167]. These systems have demonstrated reduced interfacial trap densities, enhanced energy-level alignment,and more efficient charge extraction, resulting in higher PCEs and improved operating stability in both single-junction and tandem architectures[168]. Increasing the degree of conjugation within the linker further improves charge transport across the SAM; however, this strategy must be balanced carefully, as the incorporation of excessively bulky aromatic systems introduces steric hinderance, disrupting molecular ordering and compromising monolayer stability[169].

Functionalized head group

Positioned at the interface with the perovskite layer, the head group shapes interfacial dipoles and guides crystal growth, making its strategic design paramount for optimizing both efficiency and operating stability in PSCs. The earliest application of SAMs as HTLs in PSCs involved dimethoxydiphenylamine-substituted carbazole phosphonic acids anchoring directly onto metal oxide surfaces (Fig. 4c, left)[170]. This design not only combines hole-extracting functionality with a tailored interfacial dipole, but also facilitates efficient charge transport by aligning the highest occupied molecular orbital level of the SAM with the valence band maximum of the perovskite. This work has since catalysed a wave of research focused on deliberately modifying the head group chemistry to fine-tune charge selectivity, crystallization pathways and long-term monolayer stability.

To optimize head group functionality beyond charge extraction, strategies involving Lewis bases have emerged, where terminal head groups engage uncoordinated Pb^{2+} ions at the perovskite surface. These interactions, often mediated by lone pairs on electronegative atoms such as halogens or chalcogens, passivate surface defects and suppress non-radiative recombination[171]. Additionally, such coordination can direct nucleation and the growth of larger, more uniform perovskite grains—benefits that translate into improved film morphology and enhanced performance.

Carbazole-based SAMs have arguably become one of the most prominent and extensively utilized classes of hole-transport materials in inverted PSCs[172–174]. Their performance has been improved through π-expanding the carbazole core to enhance π–π interactions and dipole moments[175–178]. Halogen substitution has also proven effective, simultaneously enhancing the interfacial dipole and passivating Pb^{2+} defects via Pb–X bonding, resulting in better energy alignment and more efficient hole extraction[179]. Motivated by the success of carbazole-based systems, other tricyclic aromatic compounds, such as phenothiazine, have emerged as promising candidates for SAMs, exhibiting similar beneficial properties in terms of hole selectivity and monolayer stability[180]. Ullah et al.[181] developed a family of SAMs incorporating chalcogen atoms (Q = O, S or Se) into the tricyclic core, leveraging heteroatom substitution to modulate interfacial energetics to align with the perovskite and passivate interfacial defects via Pb–Q Lewis acid–base interactions.

Aside from carbazole-based SAMs, triarylamine derivatives have also garnered attention as effective hole-transport SAMs. Whereas carbazoles are rigid and planar, promoting dense packing and well-aligned interfacial dipoles, non-planar triarylamines are more flexible. This flexibility can reduce monolayer order, but it also allows triarylamines to accommodate mechanical stress from the perovskite layer, helping to dissipate interfacial strain and maintain robust charge transport[182]. Modifications of the triarylamine core (for example, substituting with fluorine), along with other electron-donating groups (such as methoxy and methyl groups), enhance performance[183–185]. A notable example features a triarylamine head group and a cyanovinyl anchoring group forming an amphiphilic molecule[186]. The hydrophilic anchor ensures firm surface binding, whereas the hydrophobic head stabilizes the interface, resulting in a well-anchored monolayer and an unabsorbed overlayer, promoting superwetting behaviour that leads to exceptionally uniform perovskite films. This demonstrates how cooperative design of the SAM can yield multifunctional interfacial benefits.

Despite these advantages, the ultrathin nature and solubility of SAMs make them prone to etching during film formation and diffusion during operation, compromising interface stability. To mitigate this, polymeric and crosslinking SAMs have been developed to improve thermostability and solvent resistance by forming covalently bonded networks that reduce desorption and enhance structural integrity under stress[187–190].

Unlike heterostructure or multifunctional molecular passivation strategies, where no widely accepted baseline has yet emerged, the SAM strategy has already become a widely accepted standard for HTLs. It is now routinely employed in nearly all reported devices, whether they are single junction or tandem[191,192]. Notably, carbazole-based SAMs have delivered some of the highest reported device performances to date[100,193]; however, it remains unclear whether this reflects their intrinsic superiority or simply the fact that they are the most extensively studied and mature class of SAMs, and whether other head groups or functional modifications might achieve comparable results given further exploration and development. Future advancements in SAMs are likely to focus on simultaneously enhancing device efficiency and stability, with tailored anchoring groups, linkers and head groups providing a versatile platform to precisely control interfacial energetics, charge transport and structural integrity for high-performance devices.

Outlook

As the PCE of single-junction perovskite photovoltaics approaches that of silicon and nears its practical limit, the disparity in long-term operating stability between the two technologies becomes increasingly apparent. Bridging the performance–stability gap in perovskites requires not only the development of intrinsically more robust materials, especially in the narrow- and wide-bandgap regimens utilized in multi-junction PSCs, but also better control over interface chemistry, defect landscapes and device architectures. Oxidation of Sn in narrow-bandgap perovskite precursor solutions and bulk phases is mitigated using reductive and chelating additives, but I_2 generated at interfaces oxidizes Sn even in the absence of oxygen. The formation of I_2 at interfaces has also been linked to light-induced halide segregation in mixed-halide wide-bandgap perovskites, indicating that stable multi-junction PSCs will require a careful look at the chemical stability and defect distribution of perovskite–CTL interfaces. Even for the relatively more stable normal-bandgap perovskites, degradation under light, heat, moisture and electric field stress is often initiated or accelerated at these interfaces. As such, interfacial engineering has become central to improving long-term operational durability.

Molecular passivation, heterostructure insertion and functional SAMs have each demonstrated promise in mitigating degradation pathways originating at perovskite–CTL interfaces. Molecular passivation, albeit well established for exposed-interface passivation, remains to be thoroughly explored at the buried interface, and a more thorough understanding of the distribution of defects at specific perovskite–CTL interfaces and their effects on charge extraction would inform a rationally designed passivation strategy. Heterostructure insertion is similarly limited to the exposed interface as the solubility of 2D perovskites in 3D perovskite precursor solutions complicates buried-interface insertion. SAMs, however, are primarily limited to the buried interface, acting as HTLs in p–i–n devices, whereas effective ETL SAMs are an ongoing pursuit. Furthermore, these methods are not mutually exclusive, and concomitant passivation using multiple techniques has the potential to further benefit device performance. However, substantial work remains in the adaptation of these three methods towards scalable deposition techniques such as blade coating and slot-die coating—a necessary translation for interface passivation to be implemented at the industrial scale.

References

1. Interactive best research-cell efficiency chart. *NREL* https://www.nrel.gov/pv/interactive-cell-efficiency (2025).
2. Wang, Y. et al. Homogenized contact in all-perovskite tandems using tailored 2D perovskite. *Nature* **635**, 867–873 (2024).
3. Lin, Y. et al. A Nd@C82–polymer interface for efficient and stable perovskite solar cells. *Nature* **642**, 78–84 (2025).
4. Tan, S. et al. Spontaneous formation of robust two-dimensional perovskite phases. *Science* **388**, 639–645 (2025).
5. Zai, H. et al. Wafer-scale monolayer MoS_2 film integration for stable, efficient perovskite solar cells. *Science* **387**, 186–192 (2025).
6. Lin, R. et al. All-perovskite tandem solar cells with dipolar passivation. *Nature* **648**, 600–606 (2025).
7. Sidhik, S. et al. Deterministic fabrication of 3D/2D perovskite bilayer stacks for durable and efficient solar cells. *Science* **377**, 1425–1430 (2022).
8. Stoumpos, C. C. & Kanatzidis, M. G. The renaissance of halide perovskites and their evolution as emerging semiconductors. *Acc. Chem. Res.* **48**, 2791–2802 (2015).
9. Park, N.-G. Perovskite solar cells: an emerging photovoltaic technology. *Mater. Today* **18**, 65–72 (2015).
10. Schmidt-Mende, L. et al. Roadmap on organic–inorganic hybrid perovskite semiconductors and devices. *APL Mater.* **9**, 109202 (2021).
11. Byranvand, M. M. et al. Recent progress in mixed A-site cation halide perovskite thin-films and nanocrystals for solar cells and light-emitting diodes. *Adv. Opt. Mater.* **10**, 2200423 (2022).
12. Stoumpos, C. C., Malliakas, C. D. & Kanatzidis, M. G. Semiconducting tin and lead iodide perovskites with organic cations: phase transitions, high mobilities, and near-infrared photoluminescent properties. *Inorg. Chem.* **52**, 9019–9038 (2013).
13. Ortiz-Cervantes, C., Carmona-Monroy, P. & Solis-Ibarra, D. Two-dimensional halide perovskites in solar cells: 2D or not 2D? *ChemSusChem* **12**, 1560–1575 (2019).
14. Stoumpos, C. C. et al. Ruddlesden–Popper hybrid lead iodide perovskite 2D homologous semiconductors. *Chem. Mater.* **28**, 2852–2867 (2016).
15. Leung, T. L. et al. Stability of 2D and quasi-2D perovskite materials and devices. *Commun. Mater.* **3**, 63 (2022).
16. Maughan, A. E., Ganose, A. M., Scanlon, D. O. & Neilson, J. R. Perspectives and design principles of vacancy-ordered double perovskite halide semiconductors. *Chem. Mater.* **31**, 1184–1195 (2019).
17. Liu, C. et al. Two-dimensional perovskitoids enhance stability in perovskite solar cells. *Nature* **633**, 359–364 (2024).
18. Hadi, M. A., Islam, M. N. & Podder, J. Indirect to direct band gap transition through order to disorder transformation of $Cs_2AgBiBr_6$ via creating antisite defects for optoelectronic and photovoltaic applications. *RSC Adv.* **12**, 15461–15469 (2022).

19. Li, X. et al. Tolerance factor for stabilizing 3D hybrid halide perovskitoids using linear diammonium cations. *J. Am. Chem. Soc.* **144**, 3902–3912 (2022).
20. Gilley, I. W. et al. Combining organic cations of different sizes grants improved control over perovskitoid dimensionality and bandgap. *J. Am. Chem. Soc.* **147**, 7777–7787 (2025).
21. Yadav, C. & Kumar, S. Review on perovskite solar cells via vacuum and non-vacuum solution based methods. *Results Surf. Interfaces* **14**, 100210 (2024).
22. Zarabinia, N. & Brown, T. M. Fabrication of perovskite solar cells: a focused review on manual deposition methods. *Adv. Mater. Technol.* **10**, 2400831 (2025).
23. Chen, C. et al. Screen-printing technology for scale manufacturing of perovskite solar cells. *Adv. Sci.* **10**, 2303992 (2023).
24. Chung, T.-Y. et al. Developing screen-printing processes for silver electrodes towards all-solution coating processes for solar cells. *Polymers* **16**, 3012 (2024).
25. Liu, C. et al. Bimolecularly passivated interface enables efficient and stable inverted perovskite solar cells. *Science* **382**, 810–815 (2023).
26. Gu, H. et al. Design optimization of bifacial perovskite minimodules for improved efficiency and stability. *Nat. Energy* **8**, 675–684 (2023).
27. Deng, Y. et al. Tailoring solvent coordination for high-speed, room-temperature blading of perovskite photovoltaic films. *Sci. Adv.* **5**, eaax7537 (2019).
28. Jiao, H. et al. Perovskite grain wrapping by converting interfaces and grain boundaries into robust and water-insoluble low-dimensional perovskites. *Sci. Adv.* **8**, eabq4524 (2022).
29. Bai, Y. et al. Oligomeric silica-wrapped perovskites enable synchronous defect passivation and grain stabilization for efficient and stable perovskite photovoltaics. *ACS Energy Lett.* **4**, 1231–1240 (2019).
30. Yan, B. et al. 3D laminar flow-assisted crystallization of perovskites for square meter-sized solar modules. *Science* **388**, eadt5001 (2025).
31. Liu, J. et al. Evolutionary manufacturing approaches for advancing flexible perovskite solar cells. *Joule* **8**, 944–969 (2024).
32. Zhang, Z. et al. Suppression of phase segregation in wide-bandgap perovskites with thiocyanate ions for perovskite/organic tandems with 25.06% efficiency. *Nat. Energy* **9**, 592–601 (2024).
33. Lin, R. et al. All-perovskite tandem solar cells with 3D/3D bilayer perovskite heterojunction. *Nature* **620**, 994–1000 (2023).
34. Chen, H. et al. Regulating surface potential maximizes voltage in all-perovskite tandems. *Nature* **613**, 676–681 (2023).
35. Hao, F., Stoumpos, C. C., Chang, R. P. H. & Kanatzidis, M. G. Anomalous band gap behavior in mixed Sn and Pb perovskites enables broadening of absorption spectrum in solar cells. *J. Am. Chem. Soc.* **136**, 8094–8099 (2014).
36. Wang, T. & Yan, F. Reducing agents for improving the stability of Sn-based perovskite solar cells. *Chem. Asian J.* **15**, 1524–1535 (2020).
37. Nakamura, T. et al. Sn(IV)-free tin perovskite films realized by in situ Sn(0) nanoparticle treatment of the precursor solution. *Nat. Commun.* **11**, 3008 (2020).
38. Li-Xuan, W. et al. Limiting factors and improving solutions of p-i-n type tin-lead perovskite solar cells performance. *Acta Physica Sinica* **70**, 118402–118419 (2021).
39. Zhang, Z. et al. Mechanistic understanding of oxidation of tin-based perovskite solar cells and mitigation strategies. *Angew. Chem. Int. Ed.* **62**, e202308093 (2023).
40. Jiao, S., Wang, T. & Zhou, Z. Additive engineering toward suppression of Sn^{2+} oxidation in Sn–Pb perovskite solar cells: mechanisms, advances, and outlook. *ChemSusChem* **18**, 2500333 (2025).
41. Zhang, J. et al. Buried interface passivation of Sn–Pb narrow-bandgap perovskite for highly efficient all-perovskite tandem solar cells. *Sol. RRL* **8**, 2400184 (2024).
42. Bati, A. S. R. et al. A chemically bonded monolayer interface enables enhanced thermal stability and efficiency in Pb–Sn perovskite solar cells. *Joule* **9**, 102047 (2025).
43. Lee, H., Kang, S.B., Lee, S., Zhu, K. & Kim, D. H. Progress and outlook of Sn–Pb mixed perovskite solar cells. *Nano Converg.* **10**, 27 (2023).
44. Kulkarni, S. A. et al. Band-gap tuning of lead halide perovskites using a sequential deposition process. *J. Mater. Chem. A* **2**, 9221–9225 (2014).
45. Brennan, M. C., Ruth, A., Kamat, P. V. & Kuno, M. Photoinduced anion segregation in mixed halide perovskites. *Trends Chem.* **2**, 282–301 (2020).
46. Chen, Z., Brocks, G., Tao, S. & Bobbert, P. A. Unified theory for light-induced halide segregation in mixed halide perovskites. *Nat. Commun.* **12**, 2687 (2021).
47. Fang, Z., Nie, T., Liu, S. F. & Ding, J. Overcoming phase segregation in wide-bandgap perovskites: from progress to perspective. *Adv. Funct. Mater.* **34**, 2404402 (2024).
48. Kerner, R. A., Xu, Z., Larson, B. W. & Rand, B. P. The role of halide oxidation in perovskite halide phase separation. *Joule* **5**, 2273–2295 (2021).
49. Brivio, F., Caetano, C. & Walsh, A. Thermodynamic origin of photoinstability in the $CH_3NH_3Pb(I_{1-x}Br_x)_3$ hybrid halide perovskite alloy. *J. Phys. Chem. Lett.* **7**, 1083–1087 (2016).
50. Bischak, C. G. et al. Origin of reversible photoinduced phase separation in hybrid perovskites. *Nano Lett.* **17**, 1028–1033 (2017).
51. Cho, J., DuBose, J. T., Mathew, P. S. & Kamat, P. V. Electrochemically induced iodine migration in mixed halide perovskites: suppression through chloride insertion. *Chem. Commun.* **57**, 235–238 (2021).
52. Belisle, R. A. et al. Impact of surfaces on photoinduced halide segregation in mixed-halide perovskites. *ACS Energy Lett.* **3**, 2694–2700 (2018).
53. Li, Z. et al. Beyond the phase segregation: probing the irreversible phase reconstruction of mixed-halide perovskites. *Adv. Sci.* **9**, 2103948 (2021).
54. Mao, W. et al. Light-induced reversal of ion segregation in mixed-halide perovskites. *Nat. Mater.* **20**, 55–61 (2021).
55. Koc, F. et al. Controlling halide segregation in hybrid perovskites through varied halide stoichiometry and illumination conditions. *Adv. Electron. Mater.* **11**, 2400895 (2025).
56. Zhao, L. et al. Surface-defect-passivation-enabled near-unity charge collection efficiency in bromide-based perovskite gamma-ray spectrum devices. *Nat. Photonics* **18**, 250–257 (2024).
57. Wu, G. et al. Surface passivation using 2D perovskites toward efficient and stable perovskite solar cells. *Adv. Mater.* **34**, 2105635 (2022).
58. Fu, L. et al. Defect passivation strategies in perovskites for an enhanced photovoltaic performance. *Energy Environ. Sci.* **13**, 4017–4056 (2020).
59. Christians, J. A., Miranda Herrera, P. A. & Kamat, P. V. Transformation of the excited state and photovoltaic efficiency of $CH_3NH_3PbI_3$ perovskite upon controlled exposure to humidified air. *J. Am. Chem. Soc.* **137**, 1530–1538 (2015).
60. Isikgor, F. H. et al. Molecular engineering of contact interfaces for high-performance perovskite solar cells. *Nat. Rev. Mater.* **8**, 89–108 (2023).

61. Warby, J. et al. Understanding performance limiting interfacial recombination in pin perovskite solar cells. *Adv. Energy Mater.* **12**, 2103567 (2022).
62. Hu, J. et al. Tracking the evolution of materials and interfaces in perovskite solar cells under an electric field. *Commun. Mater.* **3**, 39 (2022).
63. Gong, C. et al. Silver coordination-induced n-doping of PCBM for stable and efficient inverted perovskite solar cells. *Nat. Commun.* **15**, 4922 (2024).
64. Jiang, Q. et al. Surface reaction for efficient and stable inverted perovskite solar cells. *Nature* **611**, 278–283 (2022).
65. Khan, J. et al. Tuning the surface-passivating ligand anchoring position enables phase robustness in $CsPbI_3$ perovskite quantum dot solar cells. *ACS Energy Lett.* **5**, 3322–3329 (2020).
66. Jiang, X. et al. Spatial conformation engineering of aromatic ketones for highly efficient and stable perovskite solar cells. *J. Am. Chem. Soc.* **146**, 34833–34841 (2024).
67. Cai, Y. et al. Multifunctional enhancement for highly stable and efficient perovskite solar cells. *Adv. Funct. Mater.* **31**, 2005776 (2021).
68. Shi, Y.-R. et al. Unraveling the role of active hydrogen caused by carbonyl groups in surface-defect passivation of perovskite photovoltaics. *Nano Energy* **97**, 107200 (2022).
69. Chen, H. et al. Improved charge extraction in inverted perovskite solar cells with dual-site-binding ligands. *Science* **384**, 189–193 (2024).
70. Zheng, J. et al. Critical role of functional groups in defect passivation and energy band modulation in efficient and stable inverted perovskite solar cells exceeding 21% efficiency. *ACS Appl. Mater. Interfaces* **12**, 57165–57173 (2020).
71. De Quilettes, D. W. et al. Impact of microstructure on local carrier lifetime in perovskite solar cells. *Science* **348**, 683–686 (2015).
72. Lin, Y. et al. π-conjugated Lewis base: efficient trap-passivation and charge-extraction for hybrid perovskite solar cells. *Adv. Mater.* **29**, 1604545 (2017).
73. Qin, P.-L. et al. Stable and efficient organo-metal halide hybrid perovskite solar cells via π-conjugated Lewis base polymer induced trap passivation and charge extraction. *Adv. Mater.* **30**, 1706126 (2018).
74. Luo, J. et al. Novel approach toward hole-transporting layer doped by hydrophobic Lewis acid through infiltrated diffusion doping for perovskite solar cells. *Nano Energy* **70**, 104509 (2020).
75. Wang, L. et al. A Eu^{3+}–Eu^{2+} ion redox shuttle imparts operational durability to Pb–I perovskite solar cells. *Science* **363**, 265–270 (2019).
76. Yang, Z. et al. Multifunctional phosphorus-containing Lewis acid and base passivation enabling efficient and moisture-stable perovskite solar cells. *Adv. Funct. Mater.* **30**, 1910710 (2020).
77. Abate, A. et al. Supramolecular halogen bond passivation of organic–inorganic halide perovskite solar cells. *Nano Lett.* **14**, 3247–3254 (2014).
78. Zhao, T., Chueh, C.-C., Chen, Q., Rajagopal, A. & Jen, A. K.-Y. Defect passivation of organic–inorganic hybrid perovskites by diammonium iodide toward high-performance photovoltaic devices. *ACS Energy Lett.* **1**, 757–763 (2016).
79. Yang, Y. et al. Amidination of ligands for chemical and field-effect passivation stabilizes perovskite solar cells. *Science* **386**, 898–902 (2024).
80. Liu, C. et al. Tuning structural isomers of phenylenediammonium to afford efficient and stable perovskite solar cells and modules. *Nat. Commun.* **12**, 6394 (2021).
81. Zhang, M. et al. Reconfiguration of interfacial energy band structure for high-performance inverted structure perovskite solar cells. *Nat. Commun.* **10**, 4593 (2019).
82. Zhang, Z. et al. Rationally designed universal passivator for high-performance single-junction and tandem perovskite solar cells. *Nat. Commun.* **16**, 753 (2025).
83. Yang, S. et al. Correction to "tailoring passivation molecular structures for extremely small open-circuit voltage loss in perovskite solar cells". *J. Am. Chem. Soc.* **142**, 11937–11938 (2020).
84. Zhou, Q. et al. Revealing steric-hindrance-dependent buried interface defect passivation mechanism in efficient and stable perovskite solar cells with mitigated tensile stress. *Adv. Funct. Mater.* **32**, 2205507 (2022).
85. Yang, S. et al. Tailoring passivation molecular structures for extremely small open-circuit voltage loss in perovskite solar cells. *J. Am. Chem. Soc.* **141**, 5781–5787 (2019).
86. Cohen, B.-E. et al. Hydroxyl functional groups in two-dimensional Dion–Jacobson perovskite solar cells. *ACS Energy Lett.* **7**, 217–225 (2022).
87. Zhao, X. et al. A charge transfer framework that describes supramolecular interactions governing structure and properties of 2D perovskites. *Nat. Commun.* **13**, 3970 (2022).
88. Choi, D. et al. Carboxyl-functionalized perovskite enables ALD growth of a compact and uniform ion migration barrier. *Joule* **9**, 101801 (2025).
89. Bi, E., Song, Z., Li, C., Wu, Z. & Yan, Y. Mitigating ion migration in perovskite solar cells. *Trends Chem.* **3**, 575–588 (2021).
90. Li, X. et al. Enhancing the stability of perovskite solar cells through cross-linkable and hydrogen bonding multifunctional additives. *J. Mater. Chem. A* **9**, 12684–12689 (2021).
91. Shi, Y. et al. (3-Aminopropyl)trimethoxysilane surface passivation improves perovskite solar cell performance by reducing surface recombination velocity. *ACS Energy Lett.* **7**, 4081–4088 (2022).
92. Bi, D. et al. Multifunctional molecular modulators for perovskite solar cells with over 20% efficiency and high operational stability. *Nat. Commun.* **9**, 4482 (2018).
93. Wu, X. et al. Efficient perovskite solar cells via surface passivation by a multifunctional small organic ionic compound. *J. Mater. Chem. A* **8**, 8313–8322 (2020).
94. Bai, Y. et al. Enhancing stability and efficiency of perovskite solar cells with crosslinkable silane-functionalized and doped fullerene. *Nat. Commun.* **7**, 12806 (2016).
95. Liu, Z. et al. Reducing perovskite/C_{60} interface losses via sequential interface engineering for efficient perovskite/silicon tandem solar cell. *Adv. Mater.* **36**, 2308370 (2024).
96. Wang, J. et al. Dipolar carbazole ammonium for broadened electric field distribution in high-performance perovskite solar cells. *J. Am. Chem. Soc.* **147**, 8663–8671 (2025).
97. Qu, Z. et al. Enhanced charge carrier transport and defects mitigation of passivation layer for efficient perovskite solar cells. *Nat. Commun.* **15**, 8620 (2024).
98. Liu, Z. et al. Grain regrowth and bifacial passivation for high-efficiency wide-bandgap perovskite solar cells. *Adv. Energy Mater.* **13**, 2203230 (2023).
99. Liu, S. et al. Buried interface molecular hybrid for inverted perovskite solar cells. *Nature* **632**, 536–542 (2024).
100. Jiang, W. et al. Toughened self-assembled monolayers for durable perovskite solar cells. *Nature* **646**, 95–101 (2025).
101. Jing, Y. et al. Interface field engineering of weakly alkaline-treated PEDOT:PSS for enhanced performance and stability of tin-based perovskite solar cells. *J. Phys. Chem. Lett.* **16**, 5258–5264 (2025).
102. Zhou, J. et al. Acidity control of interface for improving stability of all-perovskite tandem solar cells. *Adv. Energy Mater.* **13**, 2300968 (2023).
103. Shi, Y., Zhu, Z., Miao, D., Ding, Y. & Mi, Q. Interfacial dipoles boost open-circuit voltage of tin halide perovskite solar cells. *ACS Energy Lett.* **9**, 1895–1897 (2024).

104. Li, Y. et al. Polymerizable ammonium salt interlayer for efficient and stable NiO_x-based perovskite solar cells. *ACS Appl. Energy Mater.* **5**, 13062–13069 (2022).
105. Li, Y. et al. Multifunctional ionic liquid as an interfacial modifier for high-performance and stable NiO_x-based inverted perovskite solar cells. *J. Phys. Chem. Lett.* **13**, 10597–10602 (2022).
106. Wang, M. et al. Ammonium cations with high pK_a in perovskite solar cells for improved high-temperature photostability. *Nat. Energy* **8**, 1229–1239 (2023).
107. Wang, J. et al. Bilayer interface engineering through 2D/3D perovskite and surface dipole for inverted perovskite solar modules. *eScience* **4**, 100308 (2024).
108. Gharibzadeh, S. et al. Record open-circuit voltage wide-bandgap perovskite solar cells utilizing 2D/3D perovskite heterostructure. *Adv. Energy Mater.* **9**, 1803699 (2019).
109. Uzurano, G. et al. 2D/3D perovskite heterostructure solar cell with orientation-controlled Dion–Jacobson 2D phase. *Appl. Phys. Express* **16**, 041005 (2023).
110. Du, Y. et al. Manipulating the formation of 2D/3D heterostructure in stable high-performance printable $CsPbI_3$ perovskite solar cells. *Adv. Mater.* **35**, 2206451 (2023).
111. Tai, M. et al. In situ formation of a 2D/3D heterostructure for efficient and stable $CsPbI_2Br$ solar cells. *J. Mater. Chem. A* **7**, 22675–22682 (2019).
112. Yao, Q. et al. Graded 2D/3D perovskite heterostructure for efficient and operationally stable MA-free perovskite solar cells. *Adv. Mater.* **32**, 2000571 (2020).
113. Wu, T. et al. Efficient and stable tin perovskite solar cells enabled by graded heterostructure of light-absorbing layer. *Sol. RRL* **4**, 2000240 (2020).
114. Xiang, W. et al. Double perovskite interlayer stabilized highly efficient perovskite solar cells. *ACS Appl. Mater. Interfaces* **16**, 44988–44996 (2024).
115. Chen, P., He, D., Huang, X., Zhang, C. & Wang, L. Bilayer 2D–3D perovskite heterostructures for efficient and stable solar cells. *ACS Nano* **18**, 67–88 (2024).
116. Metcalf, I. et al. Synergy of 3D and 2D perovskites for durable, efficient solar cells and beyond. *Chem. Rev.* **123**, 9565–9652 (2023).
117. Hou, J. et al. Two-dimensional perovskites with maximum symmetry enable exciton diffusion length exceeding 2 micrometers. *Nat. Synth.* https://doi.org/10.1038/s44160-026-01041-4 (2026).
118. Ramakrishnan, S. et al. Phase-stabilized 2D/3D hetero-bilayers via lattice matching for efficient and stable inverted solar cells. *Joule* **9**, 101954 (2025).
119. Hou, J. et al. Synthesis of 2D perovskite crystals via progressive transformation of quantum well thickness. *Nat. Synth.* **3**, 265–275 (2024).
120. Cao, F., Zhang, P. & Li, L. Multidimensional perovskite solar cells. *Fundam. Res.* **2**, 237–253 (2022).
121. Abate, S. Y. et al. Fabrication of 1D/3D heterostructure perovskite layers by tetrabutylammonium tetrafluoroborate for high-performance devices. *Org. Electron.* **125**, 106984 (2024).
122. Ge, C. et al. Mixed dimensional perovskites heterostructure for highly efficient and stable perovskite solar cells. *Sol. RRL* **6**, 2100879 (2022).
123. Zhang, J. et al. 1D choline-PbI_3-based heterostructure boosts efficiency and stability of $CsPbI_3$ perovskite solar cells. *Angew. Chem. Int. Ed.* **62**, e202303486 (2023).
124. Zhang, Y. et al. Efficient inverted perovskite solar cells with a low-dimensional halide/perovskite heterostructure. *Adv. Energy Mater.* **12**, 2202191 (2022).
125. Meng, Y. et al. Self-assembled 1D/3D perovskite heterostructure for stable all-air-processed perovskite solar cells with improved open-circuit voltage. *ChemSusChem* **16**, e202300257 (2023).
126. Zhou, X. et al. Dimethylammonium cation-induced 1D/3D heterostructure for efficient and stable perovskite solar cells. *Molecules* **27**, 7566 (2022).
127. Zhang, J., Fan, J., Cheng, B., Yu, J. & Ho, W. Graphene-based materials in planar perovskite solar cells. *Sol. RRL* **4**, 2000502 (2020).
128. Liu, X. et al. Epitaxial 2D PbS nanosheet-formamidinium lead triiodide heterostructure enabling high-performance perovskite solar cells. *Adv. Funct. Mater.* **33**, 2304140 (2023).
129. Fahsyar, P. N. A. et al. Stabilizing high-humidity perovskite solar cells with MoS_2 hybrid HTL. *Sci. Rep.* **13**, 11996 (2023).
130. Ajdič, Ž, Jošt, M. & Topič, M. The effect of Al_2O_3 on the performance of perovskite solar cells. *Sol. RRL* **8**, 2400247 (2024).
131. Li, Q. et al. Graphene-polymer reinforcement of perovskite lattices for durable solar cells. *Science* **387**, 1069–1077 (2025).
132. Shih, M.-C. et al. A 2D/3D heterostructure perovskite solar cell with a phase-pure and pristine 2D layer. *Adv. Mater.* **37**, e2416672 (2025).
133. Szabó, G. & Kamat, P. V. How cation migration across a 2D/3D interface dictates perovskite solar cell efficiency. *ACS Energy Lett.* **9**, 193–200 (2024).
134. Chakkamalayath, J., Hiott, N. & Kamat, P. V. How stable is the 2D/3D interface of metal halide perovskite under light and heat. *ACS Energy Lett.* **8**, 169–171 (2023).
135. Chai, W. et al. Graded heterojunction improves wide-bandgap perovskite for highly efficient 4-terminal perovskite/silicon tandem solar cells. *Research* **6**, 0196 (2023).
136. Azmi, R. et al. Double-side 2D/3D heterojunctions for inverted perovskite solar cells. *Nature* **628**, 93–98 (2024).
137. Chen, B. et al. Passivation of the buried interface via preferential crystallization of 2D perovskite on metal oxide transport layers. *Adv. Mater.* **33**, 2103394 (2021).
138. Luo, L. et al. Stabilization of 3D/2D perovskite heterostructures via inhibition of ion diffusion by cross-linked polymers for solar cells with improved performance. *Nat. Energy* **8**, 294–303 (2023).
139. Li, H. et al. 2D/3D heterojunction engineering at the buried interface towards high-performance inverted methylammonium-free perovskite solar cells. *Nat. Energy* **8**, 946–955 (2023).
140. Zhang, F. et al. Engineering of conformal 2D/3D perovskite heterojunction for efficient perovskite/silicon tandem solar cells on industrially textured silicon. *Adv. Mater.* **35**, 2303139 (2023).
141. He, D. et al. Homogeneous 2D/3D heterostructured tin halide perovskite photovoltaics. *Nat. Nanotechnol.* **20**, 779–786 (2025).
142. Teale, S., Degani, M., Chen, B., Sargent, E. H. & Grancini, G. Molecular cation and low-dimensional perovskite surface passivation in perovskite solar cells. *Nat. Energy* **9**, 779–792 (2024).
143. Suo, J., Yang, B., Bogachuk, D., Boschloo, G. & Hagfeldt, A. The dual use of SAM molecules for efficient and stable perovskite solar cells. *Adv. Energy Mater.* **15**, 2400205 (2025).
144. Angus, F. J. et al. Understanding the impact of SAM Fermi levels on high efficiency p-i-n perovskite solar cells. *J. Phys. Chem. Lett.* **15**, 10686–10695 (2024).
145. Li, E. et al. Bonding strength regulates anchoring-based self-assembly monolayers for efficient and stable perovskite solar cells. *Adv. Funct. Mater.* **31**, 2103847 (2021).
146. Dai, Z. et al. Interfacial toughening with self-assembled monolayers enhances perovskite solar cell reliability. *Science* **372**, 618–622 (2021).

147. Tang, H. et al. Reinforcing self-assembly of hole transport molecules for stable inverted perovskite solar cells. *Science* **383**, 1236–1240 (2024).
148. Hubert Mutin, P., Guerrero, G. & Vioux, A. Hybrid materials from organophosphorus coupling molecules. *J. Mater. Chem.* **15**, 3761–3768 (2005).
149. Marcinko, S. & Fadeev, A. Y. Hydrolytic stability of organic monolayers supported on TiO_2 and ZrO_2. *Langmuir* **20**, 2270–2273 (2004).
150. Silverman, B. M., Wieghaus, K. A. & Schwartz, J. Comparative properties of siloxane vs phosphonate monolayers on a key titanium alloy. *Langmuir* **21**, 225–228 (2005).
151. Wan, X. et al. Thermal stability of phosphonic acid self-assembled monolayers on alumina substrates. *J. Phys. Chem. C* **124**, 2531–2542 (2020).
152. Liu, T. et al. Efficient perovskite solar modules enabled by a UV-stable and high-conductivity hole transport material. *Sci. Adv.* **11**, eadu3493 (2025).
153. Yalcin, E. et al. Monodentate versus bidentate anchoring groups in self-assembling molecules (SAMs) for robust p–i–n perovskite solar cells. *ACS Appl. Mater. Interfaces* **15**, 57153–57164 (2023).
154. Cao, Q. et al. Co-self-assembled monolayers modified NiO for stable inverted perovskite solar cells. *Adv. Mater.* **36**, 2311970 (2024).
155. Li, C. et al. Achieving 32% efficiency in perovskite/silicon tandem solar cells with bidentate-anchored superwetting self-assembled molecular layers. *Angew. Chem. Int. Ed.* **64**, e202502730 (2025).
156. Chen, N. et al. Extreme long-lifetime self-assembled monolayer for air-stable molecular junctions. *Sci. Adv.* **9**, eadh3412 (2023).
157. Li, Z. et al. Stabilized hole-selective layer for high-performance inverted p-i-n perovskite solar cells. *Science* **382**, 284–289 (2023).
158. Guo, H. et al. Efficient and stable methylammonium-free tin-lead perovskite solar cells with hexaazatrinaphthylene-based hole-transporting materials. *ACS Appl. Mater. Interfaces* **14**, 6852–6858 (2022).
159. Bejitual, T. S., Ramji, K., Kessman, A. J., Sierros, K. A. & Cairns, D. R. Corrosion of an amorphous indium tin oxide film on polyethylene terephthalate at low concentrations of acrylic acid. *Mater. Chem. Phys.* **132**, 395–401 (2012).
160. Guo, H. et al. Neglected acidity pitfall: boric acid-anchoring hole-selective contact for perovskite solar cells. *Natl Sci. Rev.* **10**, nwad057 (2023).
161. Wu, T. et al. Lattice matching anchoring of hole-selective molecule on halide perovskite surfaces for n-i-p solar cells. *Adv. Mater.* **37**, 2414576 (2025).
162. Spori, D. M. et al. Influence of alkyl chain length on phosphate self-assembled monolayers. *Langmuir* **23**, 8053–8060 (2007).
163. Timpel, M. et al. Surface modification of ZnO(0001)–Zn with phosphonate-based self-assembled monolayers: binding modes, orientation, and work function. *Chem. Mater.* **26**, 5042–5050 (2014).
164. Qu, G. et al. Conjugated linker-boosted self-assembled monolayer molecule for inverted perovskite solar cells. *Joule* **8**, 2123–2134 (2024).
165. Zhang, S. et al. Conjugated self-assembled monolayer as stable hole-selective contact for inverted perovskite solar cells. *ACS Mater. Lett.* **4**, 1976–1983 (2022).
166. Sukhorukova, P. K. et al. Triphenylamine-based interlayer with carboxyl anchoring group for tuning of charge collection interface in stabilized p-i-n perovskite solar cells and modules. *J. Power Sources* **604**, 234436 (2024).
167. Zhu, J. et al. A donor–acceptor-type hole-selective contact reducing non-radiative recombination losses in both subcells towards efficient all-perovskite tandems. *Nat. Energy* **8**, 714–724 (2023).
168. Li, C. et al. Deciphering the impact of aromatic linkers in self-assembled monolayers on the performance of monolithic perovskite/Si tandem photovoltaic. *Angew. Chem. Int. Ed.* **64**, e202420585 (2025).
169. Lefèvre, X. et al. Influence of molecular organization on the electrical characteristics of π-conjugated self-assembled monolayers. *J. Phys. Chem. C* **119**, 5703–5713 (2015).
170. Magomedov, A. et al. Self-assembled hole transporting monolayer for highly efficient perovskite solar cells. *Adv. Energy Mater.* **8**, 1801892 (2018).
171. Li, C. et al. Rational design of Lewis base molecules for stable and efficient inverted perovskite solar cells. *Science* **379**, 690–694 (2023).
172. Wang, J. et al. Self-assembled molecules for inverted $CsPbI_3$ inorganic perovskite solar cells with efficiency exceeding 20%. *Chem. Eng. J.* **508**, 160931 (2025).
173. Al-Ashouri, A. et al. Conformal monolayer contacts with lossless interfaces for perovskite single junction and monolithic tandem solar cells. *Energy Environ. Sci.* **12**, 3356–3369 (2019).
174. Li, D. et al. Co-adsorbed self-assembled monolayer enables high-performance perovskite and organic solar cells. *Nat. Commun.* **15**, 7605 (2024).
175. Wang, G. et al. Molecular engineering of hole-selective layer for high band gap perovskites for highly efficient and stable perovskite-silicon tandem solar cells. *Joule* **7**, 2583–2594 (2023).
176. Jiang, W. et al. π-expanded carbazoles as hole-selective self-assembled monolayers for high-performance perovskite solar cells. *Angew. Chem.* **134**, e202213560 (2022).
177. Zhou, J. et al. Molecular contacts with an orthogonal π-skeleton induce amorphization to enhance perovskite solar cell performance. *Nat. Chem.* **17**, 564–570 (2025).
178. Zhao, K. et al. Peri-fused polyaromatic molecular contacts for perovskite solar cells. *Nature* **632**, 301–306 (2024).
179. Yi, Z. et al. Achieving a high open-circuit voltage of 1.339 V in 1.77 eV wide-bandgap perovskite solar cells via self-assembled monolayers. *Energy Environ. Sci.* **17**, 202–209 (2024).
180. Tan, Q. et al. Inverted perovskite solar cells using dimethylacridine-based dopants. *Nature* **620**, 545–551 (2023).
181. Ullah, A. et al. Versatile hole selective molecules containing a series of heteroatoms as self-assembled monolayers for efficient p-i-n perovskite and organic solar cells. *Adv. Funct. Mater.* **32**, 2208793 (2022).
182. Yang, J. et al. Flexibility meets rigidity: a self-assembled monolayer materials strategy for perovskite solar cells. *Nat. Commun.* **16**, 6968 (2025).
183. Liao, Q. et al. Green-solvent-processable low-cost fluorinated hole contacts with optimized buried interface for highly efficient perovskite solar cells. *ACS Appl. Mater. Interfaces* **14**, 43547–43557 (2022).
184. Yalcin, E. et al. Semiconductor self-assembled monolayers as selective contacts for efficient PiN perovskite solar cells. *Energy Environ. Sci.* **12**, 230–237 (2019).
185. Wang, Y. et al. Teaching an old anchoring group new tricks: enabling low-cost, eco-friendly hole-transporting materials for efficient and stable perovskite solar cells. *J. Am. Chem. Soc.* **142**, 16632–16643 (2020).
186. Zhang, S. et al. Minimizing buried interfacial defects for efficient inverted perovskite solar cells. *Science* **380**, 404–409 (2023).
187. Wang, W. et al. Thermal cross-linking hole-transport self-assembled monolayers for perovskite solar cells. *ACS Energy Lett.* **10**, 2250–2258 (2025).

188. Ren, Z. et al. Poly(carbazole phosphonic acid) as a versatile hole-transporting material for p-i-n perovskite solar cells and modules. *Joule* **7**, 2894–2904 (2023).
189. Wang, X. et al. Regulating phase homogeneity by self-assembled molecules for enhanced efficiency and stability of inverted perovskite solar cells. *Nat. Photon.* **18**, 1269–1275 (2024).
190. Dong, B. et al. Self-assembled bilayer for perovskite solar cells with improved tolerance against thermal stresses. *Nat. Energy* **10**, 342–353 (2025).
191. Du, J. et al. Face-on oriented self-assembled molecules with enhanced π–π stacking for highly efficient inverted perovskite solar cells on rough FTO substrates. *Energy Environ. Sci.* **18**, 3196–3210 (2025).
192. Jia, L. et al. Efficient perovskite/silicon tandem with asymmetric self-assembly molecule. *Nature* **644**, 912–919 (2025).
193. Sun, Y. et al. In situ coordinated HTL strategy for high-performance and scalable perovskite solar cells. *Nat. Commun.* **16**, 9110 (2025).
194. Wu, W. et al. Stable and uniform self-assembled organic diradical molecules for perovskite photovoltaics. *Science* **389**, 195–199 (2025).

Acknowledgements

We acknowledge student support provided by the National Science Foundation under grant DGE-2234667. This work was supported by the Trienens Institute for Sustainability and Energy at Northwestern University (to M.G.K. and E.H.S.). This research was made possible by the US Department of Energy's Office of Energy Efficiency and Renewable Energy under Solar Energy Technologies Office award DE-EE0010502 (to E.H.S.).

Author contributions

J.H., I.W.G. and T.E.W. contributed equally to conceptualization and writing of the manuscript. C.L., Y.Y., B.C., M.G.K. and E.H.S. contributed to discussion and revision of the manuscript.

Competing interests

The authors declare no competing interests.

Additional information

Correspondence and requests for materials should be addressed to Bin Chen, Mercouri G. Kanatzidis or Edward H. Sargent.

Peer review information *Nature Synthesis* thanks Naeimeh Mozaffari, Nam-Gyu Park and Kelly Schutt for their contribution to the peer review of this work. Primary Handling Editor: Alexandra Groves, in collaboration with the *Nature Synthesis* team.

Reprints and permissions information is available at www.nature.com/reprints.

Publisher's note Springer Nature remains neutral with regard to jurisdictional claims in published maps and institutional affiliations.

Springer Nature or its licensor (e.g. a society or other partner) holds exclusive rights to this article under a publishing agreement with the author(s) or other rightsholder(s); author self-archiving of the accepted manuscript version of this article is solely governed by the terms of such publishing agreement and applicable law.

© Springer Nature Limited 2026